Surface freshwater storage and variability in the Amazon basin from multi-satellite observations, 1993–2007

Fabrice Papa,[1,2] Frederic Frappart,[3] Andreas Güntner,[4] Catherine Prigent,[5] Filipe Aires,[5,6] Augusto C. V. Getirana,[7] and Raffael Maurer[8]

Received 5 July 2013; revised 17 September 2013; accepted 10 October 2013; published 8 November 2013.

[1] The amount of water stored and moving through the surface water bodies of large river basins (river, floodplains, wetlands) plays a major role in the global water and biochemical cycles and is a critical parameter for water resources management. However, the spatiotemporal variations of these freshwater reservoirs are still widely unknown at the global scale. Here, we propose a hypsographic curve approach to estimate surface freshwater storage variations over the Amazon basin combining surface water extent from a multi-satellite-technique with topographic data from the Global Digital Elevation Model (GDEM) from Advance Spaceborne Thermal Emission and Reflection Radiometer (ASTER). Monthly surface water storage variations for 1993–2007 are presented, showing a strong seasonal and interannual variability, and are evaluated against in situ river discharge and precipitation. The basin-scale mean annual amplitude of ~1200 km^3 is in the range of previous estimates and contributes to about half of the Gravity Recovery And Climate Experiment (GRACE) total water storage variations. For the first time, we map the surface water volume anomaly during the extreme droughts of 1997 (October–November) and 2005 (September–October) and found that during these dry events the water stored in the river and floodplains of the Amazon basin was, respectively, ~230 (~40%) and 210 (~50%) km^3 below the 1993–2007 average. This new 15 year data set of surface water volume represents an unprecedented source of information for future hydrological or climate modeling of the Amazon. It is also a first step toward the development of such database at the global scale.

Citation: Papa, F., F. Frappart, A. Güntner, C. Prigent, F. Aires, A. C. V. Getirana, and R. Maurer (2013), Surface freshwater storage and variability in the Amazon basin from multi-satellite observations, 1993–2007, *J. Geophys. Res. Atmos.*, *118*, 11,951–11,965, doi:10.1002/2013JD020500.

1. Introduction

[2] Terrestrial waters on Earth's ice-free land represent less than 1% of the total amount of water on Earth. However, they have a crucial impact on terrestrial life and human environment, and play a major role in climate variability. Excluding ice caps, freshwater on land is stored in various reservoirs: snowpack, glaciers, aquifers and other geological formations, root zone (upper few meters of the soil), and surface waters, comprising of rivers, lakes, man-made reservoirs, wetlands, and inundated areas. These components are continuously exchanging mass with the atmosphere and the ocean by vertical and horizontal motions, and thus are an integral part of the climate system with important links and feedbacks. Moreover, analysis of the flow, spatial distribution, and storage of freshwater on land are also a key issue for understanding the terrestrial branch of the global water cycle, as well as for the management of water resources [*Chahine*, 1992; *Kundzewicz et al.*, 2007].

[3] However, although improved description of the components of the global water cycle is now recognized as being of major importance, the global distribution and spatiotemporal variations of continental water extent and volume are still poorly known [*Alsdorf et al.*, 2007a; *Papa et al.*, 2010a].

[4] Until recently, our knowledge of the spatiotemporal variations of continental waters relied on sparse in situ observations and hydrological models. In situ gauge measurements help quantify the movement of water discharge in river channels but, for instance, provide comparatively little information about the spatial dynamics of terrestrial water in floodplains and wetlands or groundwater. In addition, the availability of ground-based gauge information has dramatically decreased during the last decades [*Alsdorf and Lettenmaier*, 2003; GRDC, Global Runoff Data Base-Statistics 2012, http://

[1]Institut de Recherche pour le Developpement, IRD, LEGOS, Toulouse, France.
[2]IFCWS, Indo-French Cell for Water Sciences, IRD-IISc Joint International Laboratory Indian Institute of Science, Bangalore, India.
[3]Universite de Toulouse; UPS, OMP-GET (UPS), Toulouse, France.
[4]GFZ, German Research Centre for Geosciences, Potsdam, Germany.
[5]LERMA, CNRS, Observatoire de Paris, Paris, France.
[6]Estellus, Paris, France.
[7]Hydrological Sciences Laboratory, NASA Goddard Space Flight Center, Greenbelt, Maryland, USA.
[8]NASA Goddard Institute for Space Studies, Columbia University, New York, New York, USA.

Corresponding author: F. Papa, Institut de Recherche pour le Developpement, IRD LEGOS, Toulouse, France. (fabrice.papa@ird.fr)

2169-897X/13/10.1002/2013JD020500

www.bafg.de/GRDC/EN/01_GRDC/13_dtbse/db_stat.html?nn=201876], especially in remote areas with difficult access such as tropical regions. In some cases, public access to the latest river discharge observations can also be restricted. Lacking spatially complete measurements of inundation/wetland locations, sizes, and water volume changes, hydrologic models are unable to properly partition precipitation (minus evapotranspiration) among these several components and represent their effects on river discharge at continental-to-global scales [*Alsdorf and Lettenmaier*, 2003; *Alsdorf et al*., 2007a; *Decharme et al*., 2008, 2012; *Yamazaki et al*., 2011; *Getirana et al*., 2012]. Our ability to measure, monitor, and forecast supplies of freshwater using in situ methods and hydrological models is facing considerable difficulties, at least at large scales.

[5] The terrestrial water balance equation [*Peixoto and Oort*, 1992], as applied to a river basin, can be written as

$$P\text{–}E = Qs + Qg + \Delta V, \quad (1)$$

with P and E representing basin-averaged precipitation and evapotranspiration, respectively; Qs is river discharge; Qg is groundwater discharge across the basin boundary; and V is the total surface and subsurface storage (sum of soil moisture, snow water content, surface water storage, vegetation water content, groundwater, and glaciers [*Lettenmaier*, 2005]). In most cases, each quantity is available only with a large uncertainty [*Sheffield et al*., 2009, *Azarderakhsh et al*., 2011] and the estimation of the storage change term is particularly problematic. Given that ~60% of the world floodplains and wetlands are only inundated at some time in the year [*Matthews*, 2000], intraseasonal and interannual variations in surface-stored water volumes at regional-to-global scales are not well known and limit our ability to understand their impacts on evapotranspiration, infiltration, and runoff. With the absence of a coherent observational basis for quantifying water storage globally over long time periods, the water storage term is often ignored. However, this approach precludes consideration of surface and subsurface water volume dynamics at shorter time scales.

[6] Remote sensing techniques have been very useful to hydrology investigations especially over the last 20 years [*Smith*, 1997; *Cazenave et al*., 2004; *Alsdorf and Lettenmaier*, 2003, *Alsdorf et al*., 2007b; *Hess et al*., 2003; *Prigent et al*., 2007; *Papa et al*., 2010b; *Papa et al*., 2012a, among others].

[7] The concept of measuring the hydraulics of inland water bodies from space was first brought forth in the late 1990s based on the successes of the Topex/POSEIDON radar altimetry mission that provided the systematic monitoring of water levels of large rivers, lakes, and floodplains [*Birkett et al*., 2002; *Crétaux et al*., 2005]. Multi-satellite remote sensing techniques [e.g., *Prigent et al*., 2001, 2007, 2012; *Papa et al*., 2006, 2008a, 2010a] also offer important information on land surface waters, such as the variations of surface water extent at the global scale. Since 2002, the Gravity Recovery And Climate Experiment (GRACE) gravity mission offers, for the first time, direct estimates of the spatiotemporal variations of Total terrestrial Water Storage or TWS (the sum of ground water, soil water, surface water, and snowpack) [*Ramillien et al*., 2005; *Rodell et al*., 2007; *Tapley et al*., 2004] at seasonal and basin scales. Nevertheless, despite the increasing number of satellite observations, we still have surprisingly poor knowledge of the dynamic of surface freshwater storage at least globally and at large scale. Lacking such observations at proper space and time scales, several basic questions related to the land surface water budget are still open; perhaps the most fundamental being: How much freshwater is stored at the surface/near surface of continents? What are the spatial and temporal dynamics in terrestrial surface water storage and their link with climate variability?

[8] Recently, some efforts have been undertaken to quantify the surface freshwater storage and its variations at seasonal to interannual time scale using satellite observations. The technique, which combines surface water extent observations from a multi-satellite technique [*Papa et al*., 2010a; *Prigent et al*., 2007, 2012; the Global Inundation Extent from Multi-Satellite called hereafter (GIEMS)] and radar altimeter-derived height variations of rivers, wetlands, and inundations [*Frappart et al*., 2006], was first developed over the Rio Negro, a subbasin of the Amazon [*Frappart et al*., 2008, 2011a], and also tested over a boreal environment in the Ob River basin [*Frappart et al*., 2010a]. Using continuous water level observations derived from ENVISAT radar altimeter [*Santos da Silva et al*., 2012] between 2003 and 2007, *Frappart et al*. [2012] provide for the first time monthly variations of surface water storage for the entire Amazon basin. In particular, the results highlighted that during the 2005 exceptional drought, the amount of water stored in the river and the extensive floodplains (covering more than 300,000 km^2 or 5% of the surface of the entire basin) was ~130 km^3 (~70%) below its 2003–2007 average.

[9] The combination of GIEMS and altimeter observations has proved to be a new powerful and reliable tool for monitoring large-scale surface freshwater dynamics. However, the availability of a large sample of altimetry-derived water levels (more than 530 virtual stations for the Amazon basin case study) used in *Frappart et al*. [2012] remains an exception. Indeed, former and current radar altimeter missions, characterized by an orbit intertrack interval of ~ 80 km (ERS-1/2, ENVISAT, AltiKa) and ~ 300 km (T/P and Jason-2) at the equator, do not provide an adequate monitoring with sufficient space/time sampling of most of continental water bodies worldwide [*Biancamaria et al*., 2010; *Papa et al*., 2012b] and thus limit, at the time of writing, the development of this technique at global scale.

[10] In the present paper, we propose an innovative observation-based technique to estimate surface freshwater storage variations in rivers, floodplains, lakes, and wetlands. It combines the surface water extent from GIEMS with topographic data derived from the Global Digital Elevation Model (GDEM) from the Advance Spaceborne Thermal Emission and Reflection Radiometer (ASTER), using a hypsographic curve approach. Keeping in mind that the ultimate objective is to derive the spatial and temporal variability of freshwater storage at the global scale, the present study proposes to focus on the development of the new technique and on the analysis of the results over the Amazon River basin, the largest hydrological system of the world (~6 million km^2 of surface area), characterized by extensive floodplains and contributing with 15–20% to the total freshwater discharge to the world oceans [*Richey et al*., 1986].

[11] Section 2 will present the data sets used in this study. In section 3, focusing on the Amazon basin, we will present the methodology of the hypsographic curve approach, and

the combination of GIEMS with ASTER GDEM data set to derive surface water storage. In section 4, the results are presented and discussed over the 1993–2007 period. An evaluation is performed comparing the new estimates with other external data sets such as GRACE-derived TWS, in situ river discharge observations, and precipitation. Analysis of the results is also presented with emphasis on the two exceptional droughts of 1997 and 2005. Finally, conclusions and perspectives are discussed in section 5.

2. Data Set

2.1. Multi-Satellite-Based Surface Water Extent Dynamic

[12] The complete methodology which captures at the global scale the extent of episodic and seasonal inundations, wetlands, rivers, lakes, and irrigated agriculture is described in detail in *Prigent et al.* [2001, 2007, 2012] and *Papa et al.* [2006, 2010a]. The technique uses a complementary suite of satellite observations covering a large wavelength range: (1) Advanced Very High Resolution Radiometer (AVHRR) visible (0.58–0.68 μm) and near-infrared (0.73–1.1 μm) reflectances and the derived Normalized Difference Vegetation Index (NDVI), (2) passive microwave emissivities between 19 and 85 GHz. They are estimated from the Special Sensor Microwave/Imager (SSM/I) observations by removing the contributions of the atmosphere (water vapor, clouds, rain) and the modulation by the surface temperature [*Prigent et al.*, 1997; *Prigent et al.*, 2006]. The technique uses ancillary data from the International Satellite Cloud Climatology Project (ISCCP) [*Rossow and Schiffer*, 1999] and the National Centers for Environment Prediction (NCEP) reanalysis [*Kalnay et al.*, 1996], and (3) backscatter at 5.25 GHz from the European Remote Sensing (ERS) satellite scatterometer.

[13] Observations are averaged over each month and mapped to an equal area grid of 0.25° resolution at the equator (each pixel equals 773 km^2) [*Prigent et al.*, 2001; *Prigent et al.*, 2006]. An unsupervised classification of the three sources of satellite data is performed and the pixels with satellite signatures likely related to inundation are retained. For each inundated pixel, the monthly fractional coverage by open water is obtained using the passive microwave signal and a linear mixture model with end-members calibrated with scatterometer observations to account for the effects of vegetation cover [*Prigent et al.*, 2001, 2007]. As the microwave measurements are also sensitive to the snow cover, snow and ice masks are used to filter the results and avoid any confusion with snow-covered pixels [*Armstrong and Brodzik*, 2005]. Because the ERS scatterometer encountered serious technical problems after 2000, the processing scheme had to be adapted to extend the data set and monthly mean climatology of ERS and NDVI-AVHRR observations are used [*Papa et al.*, 2010a; *Prigent et al.*, 2012]. Fifteen years of global monthly water surfaces extent 1993–2007 is available [*Prigent et al.*, 2012]. The data set has been extensively evaluated at the global scale [*Papa et al.*, 2010a; *Prigent et al.*, 2007; *Papa et al.*, 2008a] and for a wide range of environments, including boreal regions [*Papa et al.*, 2007, 2008b] and tropical regions [*Papa et al.*, 2006; *Frappart et al.*, 2008]. This data set is intensively used for climatic and hydrological analyses, such as the evaluation of methane surface emissions models [*Bousquet et al.*, 2006; *Ringeval et al.*, 2010; *Wania et al.*, 2013] and the validation of the river flooding schemes coupled with land surface models [*Decharme et al.*, 2008, 2012; *Ringeval et al.*, 2012; *Getirana et al.*, 2012; *Pedinotti et al.*, 2012].

[14] Figure 1 shows GIEMS characteristics over the Amazon River basin (Figure 1a). Figures 1b and 1c show, respectively, the annual mean and annual maximum extent of surface water averaged over 15 years (180 months). They exhibit very realistic distributions of major rivers and tributaries (Amazonas, Solimoes, Negro) with associated inundated areas and wetlands well delineated even in complex areas characterized by extensive flooding below dense vegetation canopies, such as the Central Amazonian corridor. The spatial distribution of GIEMS over the Amazon basin was extensively evaluated against high-resolution (100 m) SAR images [*Hess et al.*, 2003] in *Prigent et al.* [2007] and in *Aires et al.* [2013], as well as using other regional surveys representing various components of wetland and open-water distributions. The evaluation led to an overall estimation of GIEMS uncertainties of ~10%. Seasonal and interannual variations of the basin-scale total surface water extent and the associated anomalies are presented in Figures 1d and 1e. The extent has a strong seasonal cycle (Figure 1d), with a mean annual averaged maximum of ~2.5×10^5 km^2 for 1993–2007. It shows a substantial interannual variability especially near the minima and maxima. The years 1997, 2002, 2006, and 2007 exhibit larger peaks (Figures 1d and 1e) mostly associated with El Niño-La Niña events. During El Niño years, the eastern part of the Amazon basin is drier than normal years, whereas the Andean catchment at medium and high elevation presents a slight increase in rainfall. During la Niña years, the southwestern parts of the Amazon basin receive more rainfall than normal years, especially in the Altiplano and high elevation regions of the Eastern Cordillera [*Espinoza et al.*, 2009; *Bookhagen and Strecker*, 2010]. The droughts of 1997 and 2005 [*Marengo et al.*, 2008a; *Tomasella et al.*, 2011; *Frappart et al.*, 2012] are also well captured.

2.2. ASTER GDEM

[15] ASTER GDEM was developed jointly by the National Aeronautic and Space Administration (NASA) and the Ministry of Economy, Trade, and Industry (METI) of Japan. The ASTER instrument, launched onboard NASA's Terra spacecraft in December 1999, has along-track stereoscopic capability using its near infrared spectral band and its nadir-viewing and backward-viewing telescopes to acquire stereo image data with a base-to-height ratio of 0.6. The basic characteristics of stereoscopy and its application to the ASTER system for GDEM generation are explained in detail in *Toutin* [2008]. The horizontal spatial resolution is 15 m and one nadir-looking ASTER visible and near-infrared (VNIR) scene corresponds to about 60 × 60 km ground area. The methodology used to produce the ASTER GDEM involves automated processing of the entire 1.5-million-scene ASTER archive acquired from the start of observation until August 2008 [*Toutin*, 2008; *Abrams et al.*, 2010]. The processing includes stereo-correlation to produce ~1,264,000 individual scene-based ASTER DEMs, cloud masking to remove cloudy pixels, stacking all cloud-screened DEMs, removing residual bad values and outliers, averaging selected data to create final pixel values, and then correcting residual anomalies. The ASTER GDEM covers land surfaces between 83°N and 83°S and is

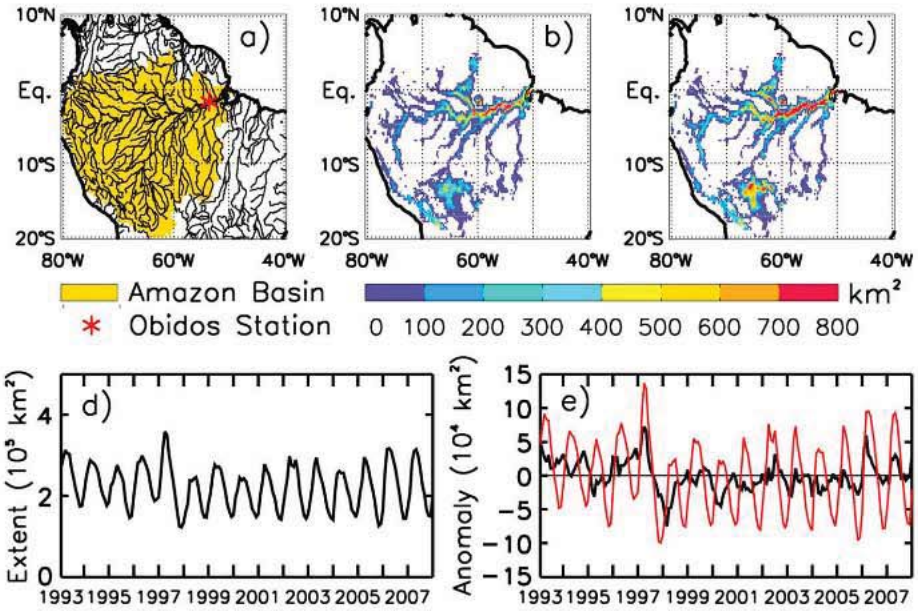

Figure 1. The global inundation extent from multi-satellite (GIEMS) and anomalies over the Amazon basin. (a) The Amazon basin and its major rivers and tributaries. The red star shows the locations of the gauging station Obidos, Para, Brazil, located 800 km upstream from the mouth of the Amazon. (b) and (c) Map of annual mean and annual maximum surface water extent averaged over 1993– 2007, for each 773 km^2 pixel. (d) Monthly mean surface water extents for 1993– 2007 for the entire Amazon basin. (e) Corresponding anomalies (by removing the mean 1993–2007 (red line) and deseasonalized obtained by subtracting the 15 year mean monthly value from individual months (black line)).

partitioned into 22,600 tiles of 1° by 1° (containing at least 0.01% of land area). ASTER GDEM has a 1 arc-second (30 m) grid of elevation and is referenced with respect to the WGS84/EGM96 geoid. Several studies have dealt with the evaluation of ASTER GDEM at local to regional scales [*Hirano et al.*, 2003; *Fujisada et al.*, 2005; *Hayakawa et al.*, 2008; *Peng et al.*, 2013]. Preproduction accuracies for the global product were estimated at ~20 m at 95% confidence level for vertical data and ~30 m at 95% confidence level for horizontal data. In this study, we use the ASTER GDEM Version 2 released in October 2011 available at http://gdem.ersdac.jspacesystems.or.jp/search.jsp.

2.3. Complementary Data for Evaluation

2.3.1. GRACE Data

[16] The Gravity Recovery And Climate Experiment mission, launched in March 2002, provides measurements of the spatiotemporal changes in Earth's gravity field. Several recent studies have shown that GRACE data over the continents can be used to derive the monthly changes of the total land water storage [*Ramillien et al.*, 2005; *Schmidt et al.*, 2008; *Landerer and Swenson*, 2012] with an accuracy of ~1.5 cm of equivalent water thickness when averaged over surfaces of a few hundred square-kilometres. In this study, we use monthly solutions from the Geo Forschung Zentrum (GFZ), the University of Texas Center for Space Research (UTCSR), and the Jet Propulsion Laboratory (JPL) from February 2003 (data are missing for January 2003) to December 2007 in order to analyze the time variations of the water mass changes in the Amazon basin. Unfortunately, the GRACE solutions suffer from the presence of an unrealistic high-frequency noise corresponding to north-south striping that is caused by orbit resonance during the Stokes coefficients determination and aliasing of poorly modelled short-term phenomena. To attenuate the noise in the Level-2 GRACE solutions, we used the global solutions postprocessing by an Independent Component Analysis (ICA) approach based on the combination of GFZ/UTCSR/JPL solutions of the same monthly period to isolate statistically independent components of the observed gravity field, and mainly the continental water storage contribution [*Frappart et al.*, 2010b, 2011b]. These data can be downloaded at: http://grgs.obs-mip.fr.

2.3.2. River Discharge

[17] Monthly discharges observed at Obidos (Figure 1a), state of Para, Brazil, which is the closest gauge to the mouth of the Amazon River (~800 km), is used in this study. The record is available at the Environmental Research Observatory (ORE) Geodynamical, hydrological, and biogeochemical control of erosion/alteration and material transport in the Amazon basin (HYBAM) website (http://www.ore-hybam.org/) over the period 1993–2007.

3. Methodology

3.1. The Hypsographic Curve Approach With ASTER GDEM

[18] The method to estimate surface freshwater storage consists of the combination of the surface water extent from GIEMS product with ASTER GDEM, using a hypsographic curve approach that relates the flooded area to the elevation. It is a three-step process (Figure 2) that can be summarized as follows:

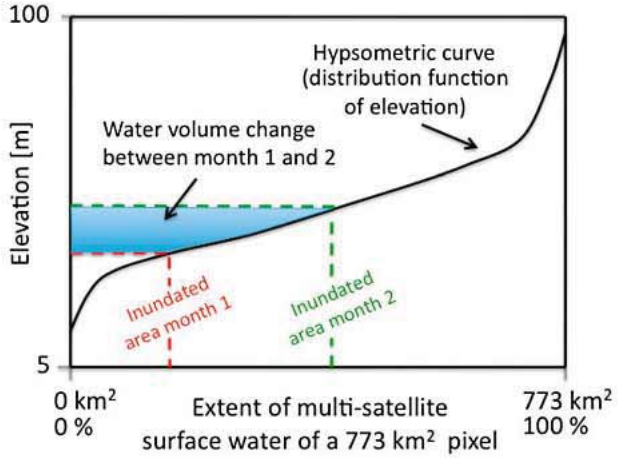

Figure 2. Schematic representation of the hypsographic curve technique to estimate surface water volume from GIEMS (see text for details).

[19] 1. For each cell of the GIEMS data set, the cumulative distribution function of elevation values is first derived from the corresponding subset of ASTER GDEM. For each pixel of the surface water extent data set (equal-area grid of 773 km^2), the corresponding subset of the ASTER GDEM is selected. Figure 3a, 3c, 3e, and 3g (left panel) shows the histograms of ASTER GDEM elevation within four pixels (equal-area grid of 773 km^2) at different locations in the Amazon basin, located in the Mamore floodplain (Figure 3a), the central Amazonian floodplain (Figure 3c), the Tapajos floodplain (Figure 3e), and the Rio Negro floodplain (Figure 3g). Approximately 800,000 elevation points of ASTER DEM fall within the satellite-derived surface water extent cell. The next step is to construct the so-called hypsographic curve, or curve of cumulative frequencies, for each cell of GIEMS data set based on ASTER GDEM elevations. The hypsographic curve is then equivalent to the distribution of elevation values in each 773 km^2 cell sorted in ascending order and represents an area-elevation relationship as illustrated in Figures 3b, 3d, 3f, and 3g (right panel) corresponding to the four locations in the Amazon basin.

[20] 2. First, for each pixel of GIEMS, a translation is applied to set to zero the lowest elevation of the hypsographic curve by subtracting the lowest value from all other elevations. The hypsographic curve is then converted into an area-surface water volume relationship by estimating the surface water volume associated with an increase of the pixel fractional open water coverage by filling the hypsographic curve from its base level to an upward level, following:

$$V(\square) = \sum_{i=1}^{\square} (h(i) - h(i-1)) \times S/100 \times i \qquad (2)$$

where V is the surface water volume (in km^3) for a percentage of flood/inundation $\square$ (a step of 1% in increment i in percentage of inundation is chosen here), S the 773 km^2 area of a GIEMS pixel, and h the elevation (in km) for a percentage of flood/inundation $\square$ given by the hypsographic curve. Examples of surface-volume profile are shown in Figure 4 for 16 locations around the Amazon basin (we will call without distinction "hypsographic curve," the area-elevation relationship as in Figure 3 or the area-volume relationship as in Figure 4).

[21] 3. Finally, in the last step, in order to estimate the surface water volume, the hypsographic curve (as in Figure 4) obtained for each grid cell of the Amazon basin is combined with the monthly variations of surface water extent from GIEMS. The surface water volume for each pixel and each month is estimated by intersecting the pixel hypsographic curve with the GIEMS estimates of pixel water coverage for that month, as shown in Figure 2. Note that, with the proposed method, the water storages below the lowest levels of storage are not accessible. Thus, the estimated water storage represents the increment above the minimum storage.

[22] Figure 4 presents, for 16 locations in the Amazon basin, the comparison between the ASTER GDEM hypsographic curves and the ones constructed by *Frappart et al.* [2012]. The hypsographic curves from *Frappart et al.* [2012] were obtained using GIEMS surface water bodies in combination with water level variations derived from ENVISAT Radar Altimeter RA-2 (processed using the Ice-1 retracker as in *Santos da Silva et al.* [2012]). Note that both hypsographic curve data sets have been derived in a totally independent way. Figure 4 clearly shows, for most cases, a very good agreement between both hypsographic curve approaches.

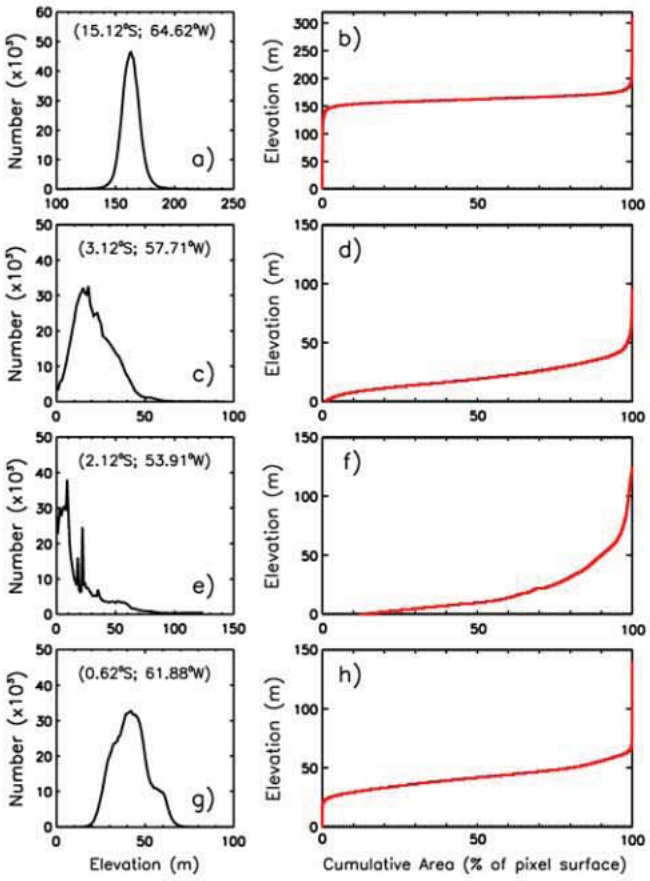

Figure 3. Examples of hypsographic curves from ASTER GDEM for the Amazon basin. Left: The histogram of ASTER GDEM elevation for a 0.25° equal grid area. Right: The hypsographic curves from ASTER GDEM, i.e., the distribution of elevation values in each 773 km^2 cell sorted in ascending order.

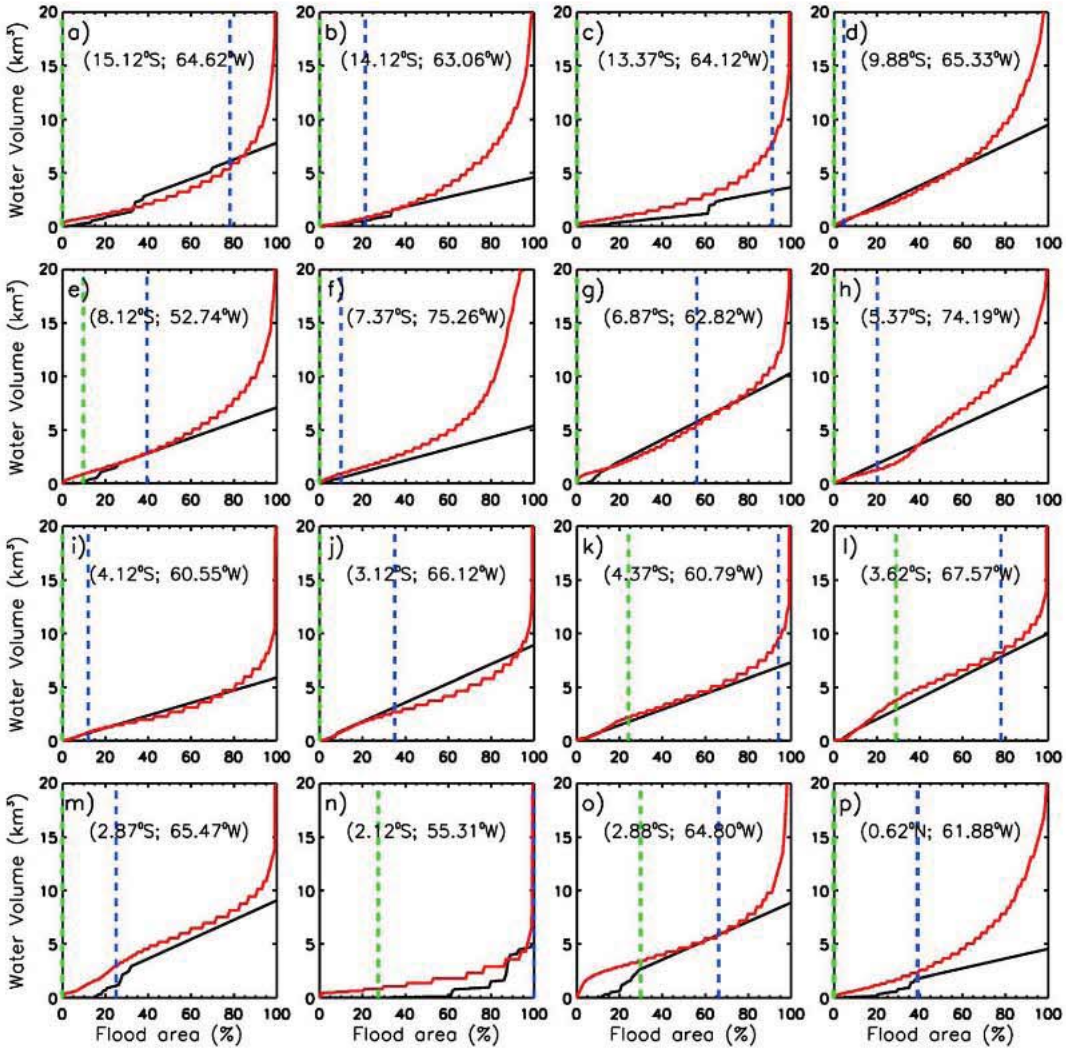

Figure 4. Surface volume profile (equivalent to the hypsographic curve), i.e., the relationship between surface water storage within each grid cell and the inundated area of a 773 km^2 pixel (in percent). Red curves are derived from ASTER GDEM and black curves are obtained using ENVISAT radar altimeter as in *Frappart et al.* [2012]. The blue (green) dashed line is the maximum (minimum) coverage of surface water observed by GIEMS during 1993–2007.

Small differences in water volume, in general less than 0.5 km^3, are observed for surface water extent covering up to 60–70% of a pixel (Figures 4a, 4c, 4d, 4e, 4j, and 4m) and up to 80–90% of a pixel (Figures 4g, 4i, 4k, 4l, and 4o). Some cases show a good agreement in the low water coverage range (<40% coverage) but a mismatch for higher flood area extent (Figures 4b, 4f, and 4h). Some cases show a larger mismatch such as in Figures 4n and 4p. However, one can notice a general behavior with ASTER GDEM hypsographic curves: potentially large fractions of surface water extent correspond to unreasonably high surface water storage (note that to make the figures comparable, the range of water volume values was limited to 20 km^3, but some values at the higher end of the curve can reach up to 100 km^3 and higher). Some cases (Figures 4a, 4c, 4e, 4g, 4i, 4j, 4k, 4l, 4m, 4n, and 4o) even show an extremely sharp increase in surface water volume for the last 20% coverage of the pixel, going from ~5 to 10 km^3 for 80–90% coverage to hundreds of km^3 for 100% of flood. This is not observed in the ENVISAT-derived hypsographic curves for which in general the maximum in surface water volume is potentially ~10 to 15 km^3. The blue and green dashed lines in Figure 4 give, respectively, the maximum and minimum surface water extent observed by GIEMS during the period 1993–2007. It shows that in most cases the sharp increase of the surface volume profile around the higher end points will not affect the estimates as such high flood extents are never reached. Nevertheless, when a large surface water extent at maximum is observed with GIEMS, such as in Figures 4c and 4k and especially Figure 4n where 100% of flooding is found in the main channel of the Amazon, it can lead to large overestimations of surface water volume. In these cases, values are jumping from ~6 km^3 at 90% to ~10 km^3 at 95% and to an unrealistic ~230 km^3 at 100% coverage of flooding for a single pixel. As a result, applying the step 3 of the methodology for all pixels of the Amazon basin leads to an unrealistic surface water volume with a mean annual amplitude of ~3500 km^3. It represents more than 1.5 times the seasonal

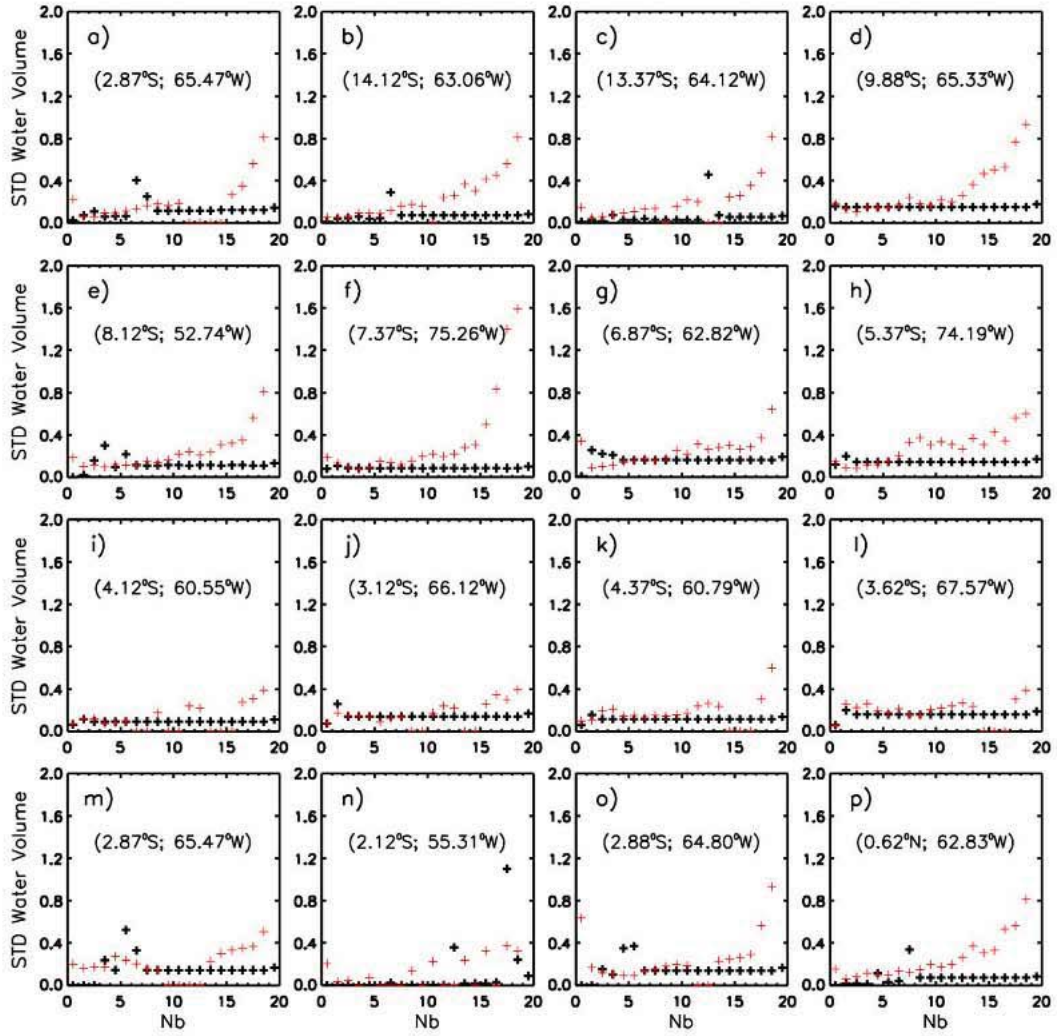

Figure 5. For the same locations as in Figure 4, the standard deviation (STD, in km^3) of the water volume derived from ASTER GDEM hypsographic curve (red plus sign) calculated over 5% flood coverage windows (20 windows named Nb on the *x* axis) calculated for each curve, see text for details). Same for ENVISAT-derived hypsographic curve with black plus sign.

amplitude measured by GRACE (~2300 km^3), composed of surface water volume, soil moisture, and root zone and groundwater storage. In *Frappart et al.* [2012], the seasonal amplitude of the Amazon surface water storage was found to be of ~1000 km^3, which lies within the same range as large-scale model simulations. For instance, *Getirana et al.* [2012] reported a seasonal amplitude of ~1100 km^3 using the Hydrological Modeling and Analysis Platform (HyMAP) model, which includes floodplain reservoirs, whereas surface water storage variations were found to be of ~470 km^3 when simulated by the WaterGAP Global Hydrology Model (WGHM) with a very simple floodplain storage module [*Güntner et al.*, 2007].

[23] The hypsographic curves showing an extremely sharp increase in surface water volume result from ASTER GDEM uncertainties and potential errors. Indeed, one of the major limitations of satellite-derived DEMs is that they are not always representing bare earth but can include vegetation and man-made structures. Moreover, because the acquisition of elevation data with ASTER is made using near infrared spectral band, GDEM can be affected by cloud cover, such as very low but dense boundary layer clouds in tropical regions. These data are difficult to filter in the raw ASTER GDEM despite large processing and can result in erroneous high elevation topographic data, inducing further large errors in the hypsographic curves.

[24] In order to avoid spurious contamination of ASTER GDEM-based surface water volumes due to high elevation values of some pixels at the upper edge of the hypsographic curve, we propose in the following a general correction of ASTER GDEM hypsographic curves.

3.2. Correction of ASTER GDEM Hypsographic Curves

[25] Figure 5 shows, for the same locations as in Figure 4, the Standard Deviation (STD) of the water volume derived from ASTER GDEM hypsographic curve (red "plus" sign) calculated over 5% flood coverage windows (20 STDs calculated for each single curve). For instance, the first plus sign represents the STD of the surface water volume calculated using the values at 1, 2, 3, 4, and 5% (first window, Nb = 1 in Figure 5), the second plus sign represents the STD calculated with the corresponding values at 6, 7, 8, 9, and 10% (second window, Nb = 2), and so on. The STD values

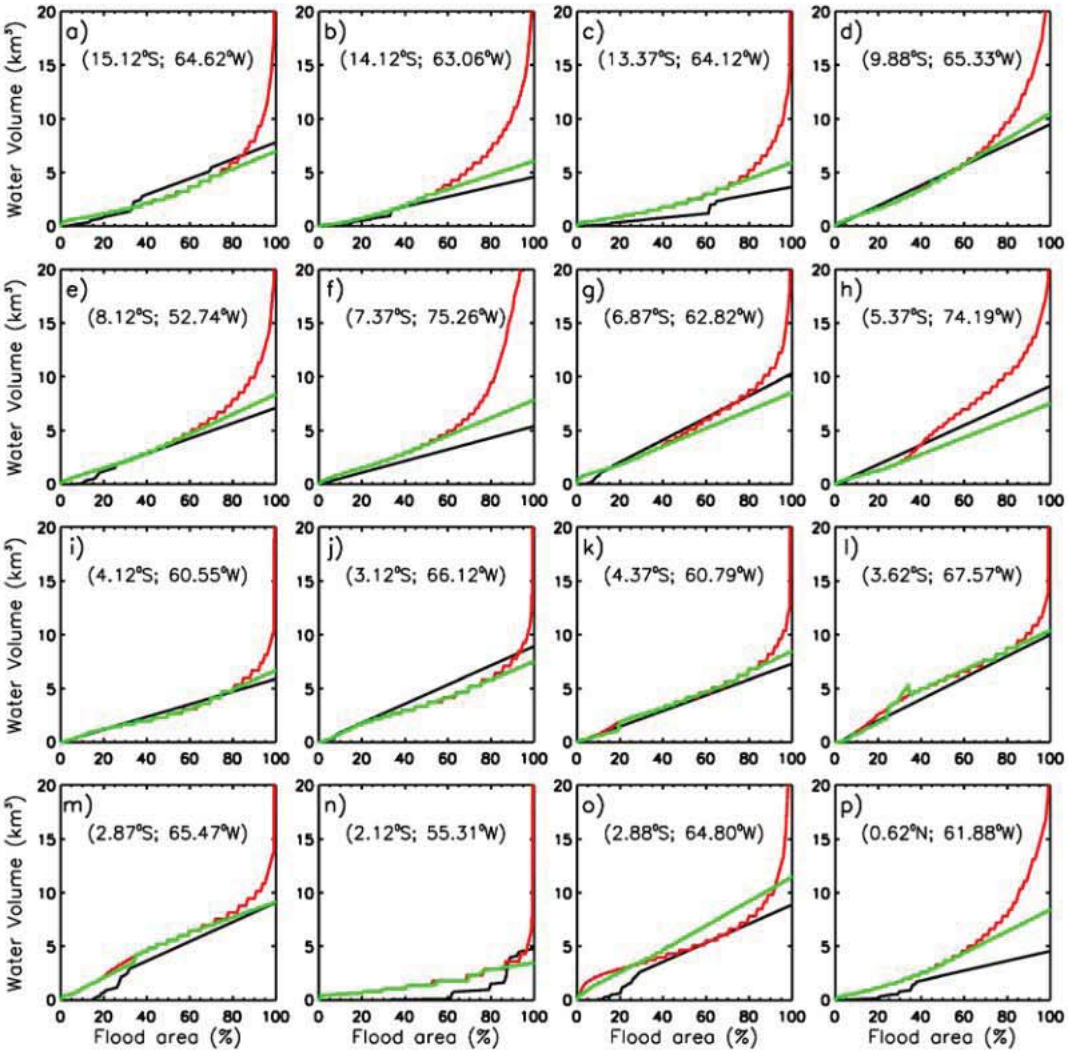

Figure 6. Examples of surface volume profile (similar as in Figure 4), i.e., the relationship between surface water storage within each grid cell and the inundated area for the Amazon basin. Red curves are derived from ASTER GDEM, black curves are obtained using ENVISAT radar altimeter as in *Frappart et al.* [2012], and green curves are derived from ASTER GDEM after correction (red curves corrected).

estimated from ENVISAT-derived hypsographic curves are also shown with a black plus sign. Figure 5 shows that in most cases, except for few isolated values, the STD calculated with ENVISAT hypsographic curves are below 0.3 km^3. It means, in other words, that within 5% of a 773 km^2 pixel, i.e., ~35 km^2, the surface water volume does not vary more than 0.3 km^3, corresponding nevertheless to water level variations of ~8.5 m at maximum. These are realistic values of volume and water level variations observed in the Amazon main channel and floodplains [*Frappart et al.*, 2006; *Santos Da Silva et al.*, 2012; *Getirana et al.*, 2012]. As expected from Figure 4, STD values calculated from ASTER GDEM hypsographic curves match well with ENVISAT values, especially for the 15 first STD values corresponding to ~75% flood coverage. However, Figure 4 also shows that for most cases, the STD values calculated from ASTER GDEM hypsographic curves for coverage above 80% are much higher than the ENVISAT ones. For ASTER GDEM, several consecutive values of STD are found between 0.6 and 1 km^3 and above. These values are mostly unrealistic as a variation of 0.8 km^3 in water volume corresponds to a water level increase of more than 22 m by 35 km^2 increment.

[26] We propose a simple procedure to correct the behavior of ASTER GDEM hypsographic curves to prevent overestimation of surface water volume at pixel level. For each percent value of flood coverage area (see Figure 4), if the value belongs to a 5% window where the STD is below a 0.4 km^3 threshold, then the corresponding surface water volume is kept. Subsequently, if the percent value belongs to a 5% window where the STD is above 0.4 km^3, the corresponding surface water volume is replaced by the fitted value based on a simple linear regression analysis using the 10 previous water volume values of the hypsographic curve. For example, a given point at 80% flood coverage, which belongs to a window with a STD more than 0.4 km^3, will be replaced by the fitted value computed using the simple linear regression equation obtained from the values between 70 and 79%.

[27] Figure 6 shows the results, for the same locations as in Figure 4, after the correction is applied to all ASTER GDEM

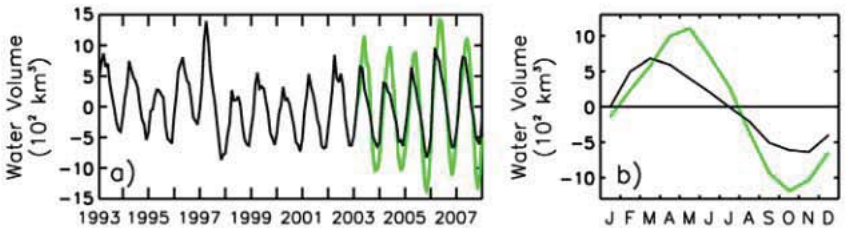

Figure 7. Surface water volume of the Amazon. (a) Monthly mean surface freshwater volume variations for 1993– 2007 for the entire Amazon basin as derived from the combination of GIEMS estimates and ASTER GDEM hypsographic curves (black curves) and compared to Total Water Storage variations estimated from GRACE (green). (b) Mean seasonal cycle (2003–2007) of Amazon surface freshwater volume variations (black) and GRACE Total Water Storage (green).

hypsographic curves (green line). It shows in most cases more realistic values even for large flood extent. For each of the 16 locations shown in Figure 6, the Root Mean Square Difference (RMSD) between ENVISAT-derived hypsographic curves and ASTER-derived original hypsographic curves ranges from 3.39 km^3 (Figure 6i) to 33.8 km^3 (Figure 6p). After correction, the RMSD between ENVISAT-derived hypsographic curves and ASTER-derived hypsographic curves is reduced and ranges between 0.34 km^3 and 1.05 km^3, respectively. For all 16 locations, the mean RMSD between ENVISAT-derived hypsographic curves and ASTER-derived original hypsographic curves is ~10.1 km^3 whereas it is ~0.62 km^3 when using ASTER-derived hypsographic curves after correction.

[28] When looking at the low end of the hypsographic curves, it should be also noted that the proposed method assumes that we cannot have access to water storage below the minimum values that ASTER GDEM (and the GIEMS) can provide. This can be a potential source of error when estimating the extreme low storage values of exceptional drought years. Indeed, in order to capture correctly the extreme low storage values during droughts, ASTER GDEM should have produced credible elevation data for those periods at the low end of the histograms. Unfortunately, it is not possible to verify such information.

4. Results, Evaluation, and Discussion

[29] Combining the corrected ASTER GDEM hypsographic curves and the GIEMS satellite-derived observations (Step 3), we can now estimate for the first time the long-term Amazon surface water storage and variations for the period 1993–2007. Figure 7 shows the monthly variations 1993–2007 (Figure 7a, 15 years) and seasonal cycle (calculated over 2003–2007, Figure 7b) of the surface water volume aggregated for the entire Amazon basin and compared to

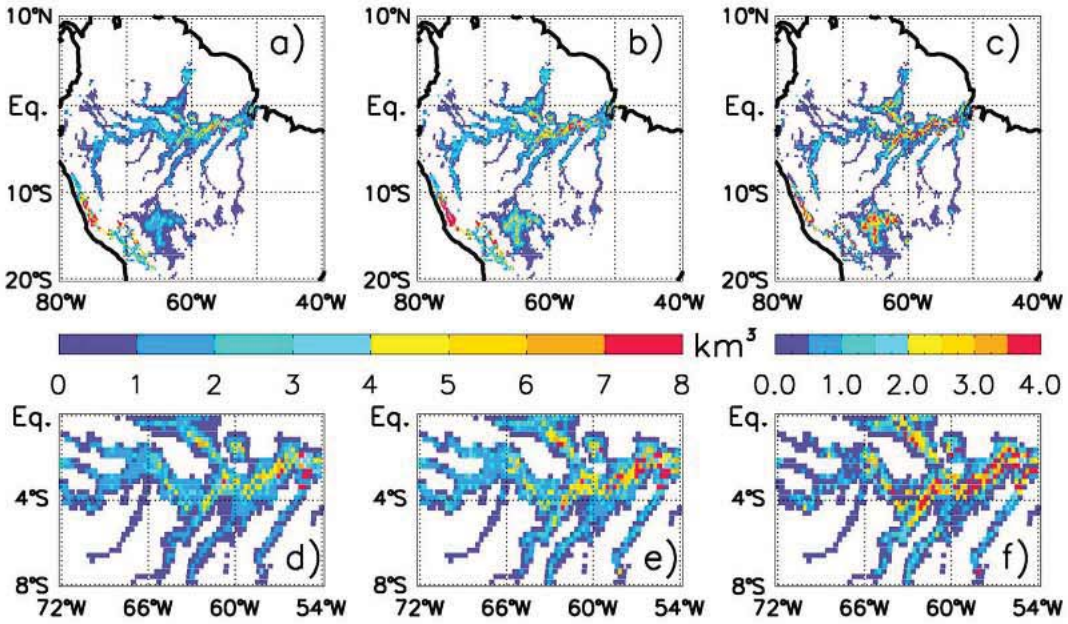

Figure 8. Maps of Amazon surface freshwater volume from 1993 to 2007. (a) Annual mean surface water volume averaged over 1993– 2007, for each 773 km^2 pixel. (b) Annual maximum surface water volume averaged over 1993– 2007. (c) The difference between the annual maximum and minimum surface water volume averaged over 1993– 2007. (d), (e) and (f) Same as Figures 8a, 8b, and 8c but zoomed over the Amazon main corridor.

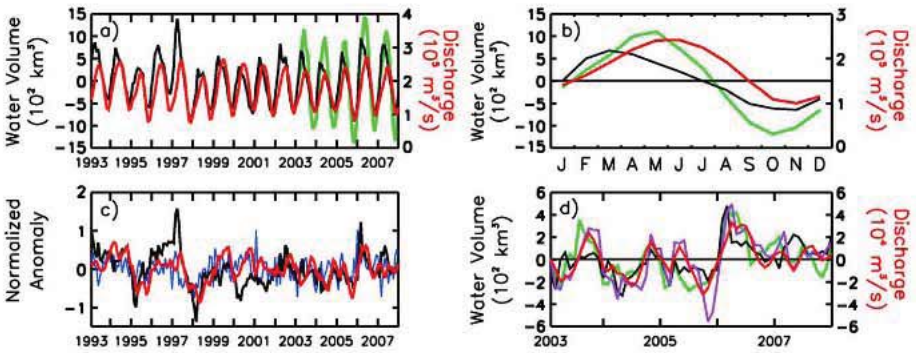

Figure 9. Correspondence among the satellite-derived monthly mean surface water storage, in situ river discharge and GRACE-based Total Water Storage in the Amazon. (a) For the entire Amazon basin, the black line is the satellite-derived surface water storage, the green line is the GRACE-based Total Water Storage, the red line is the in situ river discharge from the Brazilian Water National observed at Obidos. (b) Mean seasonal cycle (2003–2007) of Amazon surface (black) and total freshwater storage variations (green) and in situ river (red). (c) Deseasonalized normalized anomalies (obtained by subtracting the 15 year mean monthly value from individual months and dividing by the standard deviations of the raw time series) for satellite-based surface water storage (black line) and in situ river discharge (red line). The deseasonalized normalized anomalies of basin-scale mean precipitation from GPCP is also shown (blue line). (d) Corresponding deseasonalized anomalies for 2003–2007 along with the GRACE-derived total water volume change anomalies (green). The purple solid line is the deseasonalized anomalies for 2003–2007 of the surface water volume (multiply by 5 for visual purpose) aggregated over a large region [0°S–4°S; 57°W–60°W] west of Obidos location.

GRACE-derived TWS. In parallel, Figure 8 shows the spatial distribution (annual mean, annual mean maximum, and mean annual amplitude) of surface water volume for the entire basin with a focus on the Amazon central corridor.

[30] Results show a strong seasonal cycle (Figures 7a and 7b), with a mean annual amplitude of ~1200 km^3 with a maximum surface water volume observed in March, two months ahead of GRACE TWS annual peak, and a minimum value reached in November, one month after GRACE TWS minimum is recorded. This delay can be explained by the slower groundwater flow in comparison to the surface water movement, causing the 2 month delayed peak in the GRACE TWS time series. Figure 7b also shows that the surface water reservoir variation represents about 50% of the TWS variations as measured by GRACE (Figure 7b). This is in the same order of magnitude as previous accepted results on the partition of TWS into contributing hydrological storages [*Pokhrel et al.*, 2013]. For instance, using remote-sensing observations over the Rio Negro, one of the major tributaries of the Amazon River, [*Frappart et al.*, 2008; *Frappart et al.* 2011a] showed that the surface water storage contributes to 50–60% of the TWS variations. At basin scale, only results based on model simulations are available. For instance, using hydrological model outputs based on a framework combining a land surface model and a global runoff routing scheme, *Kim et al.* [2009] suggested that river storage explains ~73% of TWS variation. *Han et al.* [2009], based on simulations from Global Land Data Assimilation System (GLDAS) Noah Land Surface Model and *Alkama et al.* [2010], using the Interactions between Soil-Biosphere-Atmosphere (ISBA) land surface model, both indicated that TWS variations in the Amazon are almost equally partitioned into soil moisture and river storage variations. Modeling results from WGHM [*Güntner et al.*, 2007] suggested that surface water storage contributes to ~40% of seasonal TWS variations in the Amazon. Recently, *Paiva et al.* [2013] showed that using the new MGB-IPH model, surface waters dominate TWS for the whole Amazon area with a fraction of 56%.

[31] The new estimates of surface water storage also show a substantial interannual variability at basin scale, especially in terms of annual maximum and minimum. For instance, the years 1997, 2002, 2006, and 2007 exhibit larger peaks and the years 1997 and 2005 show more extreme minima associated with the major drought during these years (discussed later). The interannual variability for the years 2003–2007 (60 months) is also in close agreement with the interannual variations observed in the GRACE-derived TWS, with a correlation coefficient $R = 0.95$ (p-value < 0.01) and a lag-time of 2 months.

[32] In terms of spatial distribution, Figure 8 shows realistic structures with larger surface water volume and changes observed in the main Amazon channels and major tributaries (Negro, Solimoes) as well as in the South of the Amazon basin. Following the spatial distribution observed in GIEMS estimates (Figure 1), floodplains associated with major river channels are well delineated.

[33] Given the absence of other independent, large-scale, multiyear surface water volume estimates over the Amazon basin, the seasonal and interannual variability of our results over 1993–2007 are evaluated by comparison (Figure 9) with related hydrological variables, i.e., the in situ river discharge measured at Obidos (see Figure 1 for its location), basin-scale estimates of precipitation from GPCP [*Adler et al.*, 2003], and the variations of GRACE TWS (for the period 2003–2007).

[34] Showing a strong seasonal and interannual variability, Figure 9a shows that the time series of the Amazon River discharge is closely linked to the total amount of surface water volume in the whole basin. The maximum lagged correlation is of 0.90 (180 months is used to calculate the linear

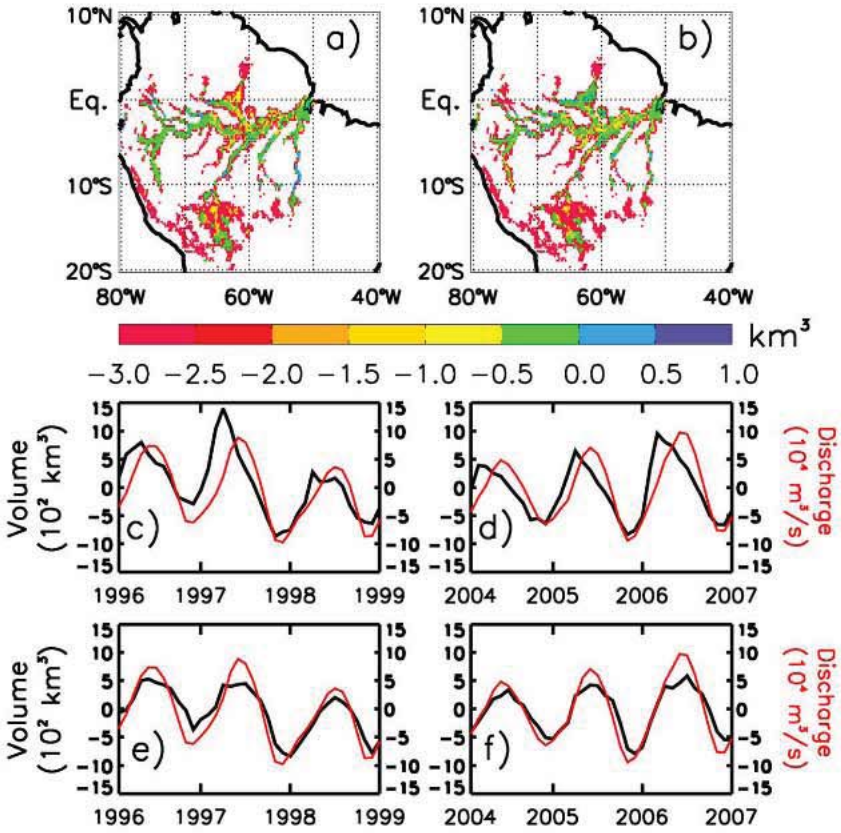

Figure 10. Major droughts in the Amazon basin during 1993–2007 as seen by the satellite-derived surface water volume anomalies and compared to in situ Amazon River observations at Obidos. (a) During October–November 1997 (averaged and relative to the mean 1993–2007). (b) During September–October 2005 (averaged and relative to the mean 1993–2007). (c–d) Corresponding 3 year anomaly time series of Amazon basin-scale surface water volume (black) and in situ river discharge at Obidos (red). (e–f) Corresponding 3 year anomaly time series of surface water volume (multiply by 10 for visual purpose) aggregated over a large region [0°S–4°S; 57°W–60°W] west of Obidos location (black) and in situ river discharge at Obidos (red).

correlation coefficient, giving $p < 0.01$, with $R > 0.14$) with the surface water volume preceding by 1 month the in situ discharge. On average (for 2003–2007), as shown by the climatology in Figure 9b, the increase and the maximum in surface water volume often precede the river discharge by 2 months. Obidos gauging station is located east of the basin, and parts of the water volume variations are first due to variations in upstream locations in the western reaches of the basin. The extensive floodplains first store and then release large amounts of water to the main rivers and consequently delay flood waves observed several days/months later in Obidos.

[35] For the entire Amazon basin and for the 1993–2007 period, the lagged correlation between the surface water volume and the basin-averaged precipitation reaches 0.86, with rain preceding the surface water volume by 2 months, and $R = 0.58$ with one month lag for the deseasonalized anomaly (computed by subtracting the 15 year mean monthly value from the monthly time series, Figure 9c). The temporal patterns between the three variables in Figure 9c are in good agreement and follow alternatively wet and dry events associated with the El Niño/La Niña phenomena. The good agreement in terms of seasonal and interannual variability between all variables is confirmed in Figure 9d during the 5 years (2003–2007) of overlapping data. The in situ river discharge, the surface water volume around Obidos (purple line), and GRACE TWS reveal the large anomalous event of the 2005 drought.

[36] The droughts that affected large areas of the Amazon basin in recent years are amongst the most severe ones in the past hundred years [*Marengo et al.*, 2008a, 2008b; *Chen et al.*, 2009; *Tomasella et al.*, 2011; *Coelho et al.*, 2012; *Frappart et al.*, 2012, 2013] with the 1997–1998, 2005, and 2010 events still considered as the most exceptional ones in the last 40 years, affecting extensive areas of more than 2 million km^2. The impact on the Amazon rainforest during these events was strong, highlighting its vulnerability to extreme drought conditions [*Philips et al.*, 2009; *Bevan et al.*, 2009]. Such events have also large potential impacts on regional biogeochemical and carbon cycles [*Philips et al.*, 2009; *Potter et al.*, 2011; *Davidson et al.*, 2012], as well as important consequences on human activities and economy.

[37] For the first time, the signatures of such phenomena on the dynamics of surface freshwater volume can be quantified directly from observations and analyzed using our new data set (Figure 9 and Figure 10). Time series in Figure 9a show the associated negative anomalies, with a large deficit in terms of surface water volume and river discharge for the

years 1997 and 2005. The spatial and temporal patterns of the droughts during these years are further illustrated in Figure 10. The drought of 1997 (Figure 10a, here October–November, the drought being in absolute value at its maximum during these two months) is characterized by large regions of negative anomaly in the south (Mamoré), North (Negro and Japura), and East (Amazon) of the basin in good agreement with observations of river discharges [*Tomasella et al.*, 2011]. The severe regional drought in the southwestern Amazon in 2005 (here September–October) is also well captured (Figure 10b), in good agreement with the spatial extent as observed in the GRACE data [*Frappart et al.*, 2012]. For both years, the monthly evolution of surface water volume, at basin scale (Figures 10c and 10d) and for the region around the gauging station Obidos (Figures 10e and 10f), show a close correspondence with the in situ river discharge, indicating a similar deficit for the same period. During October–November 1997, the amount of surface water stored in the entire Amazon basin was about ~230 km^3 (or 38%) below the October–November 1993–2007 average. A deficit of ~210 km^3 (or 48%) for September–October 2005 is found, a little bit less than half the GRACE-observed TWS deficiency of ~500 km^3 as given by *Chen et al.* [2009]. In the region west of Obidos [0°S–4°S; 57°W–60°W], these deficit values can reach up to 60% in 1997 and 73% in 2005, in good agreement with the estimates (70%) from *Frappart et al.* [2012]. Investigating the causes and impacts of these anomalous events in the Amazon is far beyond the scope of this paper, but the new availability of these long-term continuous estimates of surface water volume will help such future studies.

5. Conclusion and Perspectives

[38] This study presents the first observation-based data set that quantifies for the entire Amazon basin the monthly distribution and variation of surface freshwater storage at ~25 km sampling intervals over more than a decade, 1993–2007. The method is based on a hypsographic curve approach combining surface water extent from a multi-satellite technique (GIEMS) with topographic data from ASTER GDEM. It is a three-step process where, to summarize, cumulative distribution functions of elevation and surface-volume profiles are derived from ASTER GDEM and combined with the monthly variations of pixel water coverage from GIEMS in order to derive surface freshwater volume. Prior to the last step, an evaluation of ASTER GDEM hypsographic curves is performed with the hypsographic curves derived from ENVISAT-radar altimeter. And an adequate correction is applied to ASTER GDEM database to avoid water volume overestimations. The new estimates of monthly surface freshwater volume show realistic spatial structures. The temporal variations that are associated show a strong seasonal cycle and interannual variability. The basin-scale mean annual amplitude of ~1200 km^3 contributes to about half of the variations of GRACE-derived TWS. Monthly surface water storage variations for 1993–2007 are evaluated against other related hydrological variables such as in situ river discharge, precipitation and GRACE observations, showing that the seasonal and interannual variations agree well within all variables. Finally, we show that the new data set captures well the two extreme droughts observed in 1997 and 2005 and helps to quantify the water deficit during that period. The amount of surface water stored in the entire Amazon basin during October–November 1997 was about ~230 km^3 (or 38%) below the October–November 1993–2007 average while it reached a deficit of ~210 km^3 (or 48%) for September–October 2005, about half the GRACE-observed deficiency of ~500 km^3 of TWS in the entire basin for that period.

[39] ASTER GDEM, and global satellite-derived DEMs in general, such as SRTM30 DEM for instance, show a series of characteristics, artifacts, and anomalies that can cause significant problems or errors when used for hydrological applications [*Valeriano et al.*, 2006; *Yamazaki et al.*, 2012]. Some typical problems include the influence of vegetation cover and man-made constructions. In ASTER GDEM, the acquisition of elevation data using near infrared spectral band can introduce errors due to cloud cover, such as very low but dense boundary layer clouds in tropical regions. In areas of low relief, these small deviations from the true surface elevation can cause errors that are difficult to filter when representing the true river and floodplain profiles. These effects may create artificial islands in the floodplain likely to introduce inaccurate elevation in the DEM with consequences on the hypsographic curve technique. Moreover, in order to capture correctly the extreme low storage values during droughts, ASTER GDEM should have produced credible elevation data for those periods at the low end of the hypsographic curves. Such information is difficult to verify. In order to improve the performance of DEMs for hydrological applications, a few attempts have been proposed in the literature to reduce their uncertainty [*Wilson et al.*, 2007; *Coe et al.*, 2008]. However, DEM errors remain as one of the main sources of uncertainty in understanding and quantifying the interactions between rivers and floodplains. On a large to global scale, due to the regional variations in the type of errors, no method still exists that addresses all possible problems. These issues should be investigated in future studies.

[40] This unique data set of Amazon surface freshwater volume variations over 15 years (to be updated until present in a near future when global land surface emissivities become available) removes a crucial obstacle to progress on several fundamental scientific questions and can now be used to improve our understanding of hydrological and climate processes in the Amazon region.

[41] For instance, as proposed in *Frappart et al.* [2011a] over the Rio Negro, the surface freshwater storage, together with soil moisture products, can be used to separate the integral GRACE signal into the contributions of individual storage components and isolate the variations of groundwater storage. Such results would also help to estimate for the first time the groundwater recharge in the entire Amazon basin. Bringing together these variables with river discharge measurements, rainfall and surface evaporation estimates in an integrated approach will also yield improved overall knowledge of the different components of the Amazon terrestrial water budget. For instance, *Azarderakhsh et al.* [2011] demonstrate the importance to integrate the behavior of surface water dynamics when investigating and characterizing the closure of the Amazon water budget and its link to natural climate variability. In addition, this new 15 year data set of surface water volume over the Amazon represents an unprecedented source of information for future hydrological or

climate modeling of the region. In particular, it will help to better characterize and understand the processes during extreme events such as exceptional droughts and floods. Moreover, it will play a key role in the definition and validation of future hydrology-oriented satellite missions such as SWOT (Surface Water and Ocean Topography).

[42] Finally, as GIEMS and ASTER are available globally, this study is also a first step toward the development of such database at the global scale. A global surface freshwater volume data set is crucial to understand the role of continental water in the global water cycle, as well as in the present sea level rise. Although progress has been made on quantifying the two primary contributors to sea level rise, namely thermal expansion due to ocean warming and melting glaciers and ice sheets, large uncertainties remain regarding the effect of changes in continental water storage, despite recent important results from GRACE. The future estimates of global surface freshwater volume will give the opportunity to better quantify fluctuations in freshwater flux to the ocean, and will help better understanding the role of terrestrial water in the present sea level rise and variability [*Ramilien et al.*, 2008; *Milly et al.*, 2010; *Pokhrel et al.*, 2012].

[43] **Acknowledgments.** This work was supported by the CNES TOSCA and OSTST grants "Variability of terrestrial freshwater storage in the Tropics from multi-satellite observations" managed by S. Cherchali and by NASA's NEWS grant NNDX7AO90E managed by Jared K. Entin. We thank Robert Dickinson and two anonymous reviewers for their constructive comments and suggestions.

References

Abrams, M., B. Bailey, H. Tsu, and M. Hato (2010), The ASTER Global DEM, *Photogramm. Eng. Remote Sens.*, *76*, 344–348.

Adler, R. F., et al. (2003), The Version 2 Global Precipitation Climatology Project (GPCP) monthly precipitation analysis 1979-present, *J. Hydrometeorol.*, *4*, 1147–1167.

Aires, F., F. Papa, and C. Prigent (2013), A long-term, high-resolution wetland dataset over the Amazon basin, downscaled from a multi-wavelength retrieval using SAR, *J. Hydrometeorol.*, *14*, 594–607, doi:10.1175/JHM-D-12-093.1.

Alkama, R., B. Decharme, H. Douville, M. Becker, A. Cazenave, J. Sheffield, A. Voldoire, S. Tyteca, and P. Le Moigne (2010), Global evaluation of the ISBA-TRIP continental hydrologic system, *J. Hydrometeorol.*, *11*(3), 583–600.

Alsdorf, D. E., and D. P. Lettenmaier (2003), Tracking fresh water from space, *Science*, *301*, 1492–1494.

Alsdorf, D. E., E. Rodríguez, and D. P. Lettenmaier (2007a), Measuring surface water from space, *Rev. Geophys.*, *45*, RG2002, doi:10.1029/2006RG000197.

Alsdorf, D., P. Bates, J. Melack, M. Wilson, and T. Dunne (2007b), Spatial and temporal complexity of the Amazon flood measured from space, *Geophys. Res. Lett.*, *34*, L08402, doi:10.1029/2007GL029447.

Armstrong, R. L., and M. J. Brodzik (2005), *Northern Hemisphere EASE-Grid Weekly Snow Cover and Sea Ice Extent Version 3*, National Snow and Ice Data Center, Boulder, Colorado USA.

Azarderakhsh, M., W. B. Rossow, F. Papa, H. Norouzi, and R. Khanbilvardi (2011), Diagnosing water variations within the Amazon basin using satellite data, *J. Geophys. Res.*, *116*, D24107, doi:10.1029/2011JD015997.

Bevan, S. L., P. R. J. North, W. M. F. Grey, S. O. Los, and S. E. Plummer (2009), Impact of atmospheric aerosol from biomass burning on Amazon dry-season drought, *J. Geophys. Res.*, *114*, D09204, doi:10.1029/2008JD011112.

Biancamaria, S., K. M. Andreadis, M. Durand, E. A. Clark, E. Rodriguez, N. M. Mognard, D. E. Alsdorf, D. P. Lettenmaier, and Y. Oudin (2010), Preliminary characterization of SWOT hydrology error budget and global capabilities, *IEEE J. Sel. Topics Appl. Earth Obs. Remote Sens.*, *3*(1), 6–19.

Birkett, C. M., L. A. K. Mertes, T. Dunne, M. H. Costa, and M. J. Jasinski (2002), Surface water dynamics in the Amazon Basin: Application of satellite radar altimetry, *J. Geophys. Res.*, *107*(D20), 8059, doi:10.1029/2001JD000609.

Bookhagen, B., and M. R. Strecker (2010), Modern Andean rainfall variation during ENSO cycles and its impact on the Amazon Basin, in Neogene history of Western Amazonia and its significance for modern diversity, in *Amazonia, Landscape and Species Evolution: A Look Into the Past*, edited by C. Hoorn, H. Vonhof, and F. Wesselingh, pp. 223–241, Blackwell, Oxford.

Bousquet, P., et al. (2006), Contribution of anthropogenic and natural sources to atmospheric methane variability, *Nature*, *443*, 439–443, doi:10.1038/nature05132.

Cazenave, A., P. C. D. Milly, H. Douville, J. Benveniste, P. Kosuth, and D. P. Lettenmaier (2004), Space techniques used to measure change in terrestrial waters, *Eos Trans. AGU*, *85*(6), 59–59.

Chahine, M. (1992), The hydrological cycle and its influence on climate, *Nature*, *359*, 373–380.

Chen, J. L., C. R. Wilson, B. D. Tapley, Z. L. Yang, and G. Y. Niu (2009), 2005 drought event in the Amazon River basin as measured by GRACE and estimated by climate models, *J. Geophys. Res.*, *114*, B05404, doi:10.1029/2008JB006056.

Coe, M. T., M. H. Costa, and E. A. Howard (2008), Simulating the surface waters of the Amazon River basin: Impacts of new river geomorphic and flow parameterization, *Hydrol. Processes*, *22*, 2542–2553, doi:10.1002/hyp.6850.

Coelho, C. A. S., I. A. F. Cavalcanti, S. M. S. Costa, S. R. Freitas, E. R. Ito, G. Luz, A. F. Santos, C. A. Nobre, J. A. Marengo, and A. B. Pezza (2012), Climate diagnostics of three major drought events in the Amazon and illustrations of their seasonal precipitation predictions, *Meteorol. Appl.*, *19*, 237–255, doi:10.1002/met.1324.

Crétaux, J. F., A. V. Kouraev, F. Papa, M. Bergé-Nguyen, A. Cazenave, N. Aladin, and I. S. Plotnikov (2005), Evolution of sea level of the big Aral Sea from satellite altimetry and its implications for water balance, *J. Great Lakes Res.*, *31*, 520–534.

Davidson, E. A., et al. (2012), The Amazon basin in transition, *Nature*, *481*, 321–328, doi:10.1038/nature10717.

Decharme, B., H. Douville, C. Prigent, F. Papa, and F. Aires (2008), A new river flooding scheme for global climate applications: Off-line validation over South America, *J. Geophys. Res.*, *113*, D11110, doi:10.1029/2007JD009376.

Decharme, B., R. Alkama, F. Papa, S. Faroux, H. Douville, and C. Prigent (2012), Global off-line evaluation of the ISBA-TRIP flood model, *Clim. Dyn.*, *38*(7-8), 1389–1412, doi:10.1007/s00382-011-1054-9.

Espinoza, J. C., J. Ronchail, J. L. Guyot, G. Cocheneau, N. Filizola, W. Lavado, E. de Oliveira, R. Pombosa, and P. Vauchel (2009), Spatio – Temporal rainfall variability in the Amazon Basin Countries (Brazil, Peru, Bolivia, Colombia and Ecuador), *Int. J. Climatol.*, *29*, 1574–1594.

Frappart, F., S. Calmant, M. Cauhopé, F. Seyler, and A. Cazenave (2006), Preliminary results of ENVISAT RA-2 derived water levels validation over the Amazon basin, *Remote Sens. Environ.*, *100*, 252–264.

Frappart, F., F. Papa, J. S. Famiglietti, C. Prigent, W. B. Rossow, and F. Seyler (2008), Interannual variations of river water storage from a multiple satellite approach: A case study for the Rio Negro River basin, *J. Geophys. Res.*, *113*, D21104, doi:10.1029/2007JD009438.

Frappart, F., F. Papa, A. Güntner, S. Werth, G. Ramillien, C. Prigent, W. B. Rossow, and M.-P. Bonnet (2010a), Interannual variations of the terrestrial water storage in the Lower Ob' Basin from a multisatellite approach, *Hydrol. Earth Syst. Sci.*, *14*, 2443–2453, doi:10.5194/hess-14-2443-2010.

Frappart, F., G. Ramillien, P. Maisongrande, and M.-P. Bonnet (2010b), Denoising satellite gravity signals by Independent Component Analysis, *IEEE Geosci. Remote Sens. Lett.*, *7*(3), 421–425, doi:10.1109/LGRS.2009.2037837.

Frappart, F., et al. (2011a), Satellite-based estimates of groundwater storage variations in large drainage basins with extensive floodplains, *Remote Sens. Environ.*, *115*, 1588–1594, doi:10.1016/j.rse.2011.02.003.

Frappart, F., G. Ramillien, M. Leblanc, S. O. Tweed, M.-P. Bonnet, and P. Maisongrande (2011b), An independent Component Analysis approach for filtering continental hydrology in the GRACE gravity data, *Remote Sens. Environ.*, *115*(1), 187–204, doi:10.1016/j.rse.2010.08.017.

Frappart, F., F. Papa, J. Santos da Silva, G. Ramillien, C. Prigent, F. Seyler, and S. Calmant (2012), Surface freshwater storage and dynamics in the Amazon basin during the 2005 exceptional drought, *Environ. Res. Lett.*, *7*, 044010, 7, doi:10.1088/1748-9326/7/4/044010.

Frappart, F., G. Ramillien, and J. Ronchail (2013), Changes in terrestrial water storage versus rainfall and discharges in the Amazon basin, *Int. J. Clim.*, doi:10.1002/joc.3647.

Fujisada, H., G. B. Bailey, G. G. Kelly, S. Hara, and M. J. Abrams (2005), ASTER DEM Performance, *IEEE Trans. Geosci. Remote Sens.*, *43*, 2707–13.

Getirana, A., A. Boone, D. Yamazaki, B. Decharme, F. Papa, and N. Mognard (2012), The Hydrological Modeling and Analysis Platform

(HyMAP): Evaluation in the Amazon basin, *J. Hydrometeorol.*, *13*, 1641–1665, doi:10.1175/JHM-D-12-021.1.

Güntner A., J. Stuck, S. Werth, P. Döll, K. Verzano, and B. Merz (2007), A global analysis of temporal and spatial variations in continental water storage, *Water Resour. Res.*, *43*, W05416, doi:10.1029/2006WR005247.

Han, S.-C., H. Kim, I.-Y. Yeo, P. Yeh, T. Oki, K.-W. Seo, D. Alsdorf, and S. B. Luthcke (2009), Dynamics of surface water storage in the Amazon inferred from measurements of inter-satellite distance change, *Geophys. Res. Lett.*, *36*, L09403, doi:10.1029/2009GL037910.

Hayakawa, Y. S., T. Oguchi, and Z. Lin (2008), Comparison of New and Existing Global Digital Elevation Models: ASTER G-DEM and SRTM-3, *Geophys. Res. Lett.*, *35*, L17404, doi:10.1029/2008GL035036.

Hess, L. L., J. M. Melack, E. M. L. M. Novob, C. C. F. Barbosac, and M. Gastil (2003), Dual-season mapping of wetland inundation and vegetation for the central Amazon basin, *Remote Sens. Environ.*, *87*, 404–428.

Hirano, A., R. Welch, and H. Lang (2003), Mapping from ASTER Stereo Image Data: DEM Validation and Accuracy Assessment, *ISPRS J. Photogramm. Remote Sens.*, *57*, 356–370.

Kalnay, E., et al. (1996), The NCEP/NCAR 40-year reanalysis project, *Bull. Am. Meteorol. Soc.*, *77*, 437–470.

Kim, H., P. J.-F. Yeh, T. Oki, and S. Kanae (2009), Role of rivers in the seasonal variations of terrestrial water storage over global basins, *Geophys. Res. Lett.*, *36*, L17402, doi:10.1029/2009GL039006.

Kundzewicz, Z. W., L. J. Mata, N. W. Arnell, P. Döll, P. Kabat, B. Jiménez, K. A. Miller, T. Oki, Z. Sen, and I. A. Shiklomanov (2007), Freshwater resources and their management, in *Climate Change 2007: Impacts, Adaptation, and Vulnerability. Contribution of Working Group II to the Fourth Assessment Report of the Intergovernmental Panel on Climate Change*, edited by M. L. Parry et al., pp. 173–210, Cambridge Univ. Press, Cambridge.

Landerer, F. W., and S. C. Swenson (2012), Accuracy of scaled GRACE terrestrial water storage estimates, *Water Resour. Res.*, *48*, W04531, doi:10.1029/2011WR011453.

Lettenmaier, D. P. (2005), Observations of the global water cycle—Global monitoring networks, in *Encyclopedia of Hydrologic Sciences*, vol. *5*, edited by M. G. Anderson and J. J. McDonnell, pp. 2719–2732, John Wiley, Hoboken, N. J.

Marengo, J. A., C. A. Nobre, J. Tomasella, M. D. Oyama, G. S. Oliveira, R. de Oliveira, H. Camargo, L. M. Alves, and I. F. Brown (2008a), The drought of Amazonia in 2005, *J. Clim.*, *21*, 495–516.

Marengo, J. A., C. A. Nobre, J. Tomasella, M. F. Cardoso, and M. D. Oyama (2008b), Hydroclimatic and ecological behaviour of the drought of Amazonia in 2005, *Philos. Trans. R. Soc. London B*, *363*, 1773–1778.

Matthews, E. (2000), *Wetlands in Atmospheric Methane: Its Role in the Global Environment*, edited by M. A. K. Khalil, pp. 202–233, Springer-Verlag, New York.

Milly, P. C. C., A. Cazenave, J. S. Famiglietti, V. Gornitz, K. Laval, D. P. Lettenmaier, D. L. Sahagian, J. M. Wahr, and C. R. Wilson (2010), Terrestrial water-storage contributions to sea-level rise and variability, in *Understanding Sea-Level Rise and Variability*, edited by J. A. Church et al., pp. 226–255, Wiley Blackwell, Oxford, UK.

Paiva, R. C. D., D. C. Buarque, W. Collischonn, M.-P. Bonnet, F. Frappart, S. Calmant, and C. A. B. Mendes (2013), Largescale hydrologic and hydrodynamic modeling of the Amazon River basin, *Water Resour. Res.*, *49*, 1226–1243, doi:10.1002/wrcr.20067.

Papa, F., C. Prigent, F. Durand, and W. B. Rossow (2006), Wetland dynamics using a suite of satellite observations: A case study of application and evaluation for the Indian Subcontinent, *Geophys. Res. Lett.*, *33*, L08401, doi:10.1029/2006GL025767.

Papa, F., C. Prigent, and W. B. Rossow (2007), Ob' River flood inundations from satellite observations: A relationship with winter snow parameters and river runoff, *J. Geophys. Res.*, *112*, D18103, doi:10.1029/2007JD008451.

Papa, F., C. Prigent, and W. B. Rossow (2008a), Monitoring flood and discharge variations in the large Siberian rivers from a multi-satellite technique, *Surv. Geophys.*, *29*(4-5), 297–317, doi:10.1007/s10712-008-9036-0.

Papa, F., A. Güntner, F. Frappart, C. Prigent, and W. B. Rossow (2008b), Variations of surface water extent and water storage in large river basins: A comparison of different global data sources, *Geophys. Res. Lett.*, *35*, L11401, doi:10.1029/2008GL033857.

Papa, F., C. Prigent, W. B. Rossow, and E. Matthews (2010a), Interannual variability of surface water extent at global scale, 1993-2004, *J. Geophys. Res.*, *115*, D12111, doi:10.1029/2009JD012674.

Papa, F., F. Durand, W. B. Rossow, A. Rahman, and S. K. Bala (2010b), Satellite altimeter-derived monthly discharge of the Ganga-Brahmaputra River and its seasonal to interannual variations from 1993 to 2008, *J. Geophys. Res.*, *115*, C12013, doi:10.1029/2009JC006075.

Papa, F., S. K. Bala, R. Kumar Pandey, F. Durand, V. V. Gopalakrishna, A. Rahman, and W. B. Rossow (2012a), Ganga-Brahmaputra river discharge from Jason-2 radar altimetry: An update to the long-term satellite-derived estimates of continental freshwater forcing flux into the Bay of Bengal, *J. Geophys. Res.*, *117*, C11021, doi:10.1029/2012JC008158.

Papa, F., S. Biancamaria, C. Lion, and W. B. Rossow (2012b), Uncertainties in mean river discharge estimates associated with satellite altimeters temporal sampling intervals a case study for the annual peak flow in the context of the future SWOT hydrology mission, *IEEE Geosci. Remote Sens. Lett*, *9*(4), 569–573, doi:10.1109/LGRS.2011.2174958.

Pedinotti, V., A. Boone, B. Decharme, J. F. Cretaux, N. Mognard, G. Panthou, F. Papa, and B. A. Tanimoun (2012), Evaluation of the ISBA-TRIP continental hydrologic system over the Niger basin using in situ and satellite derived datasets, *Hydrol. Earth Syst. Sci.*, *16*, 1745–1773, doi:10.5194/hess-16-1745-2012.

Peixoto, J. P., and A. H. Oort (1992), *Physics of Climate*, Am. Inst. of Phys. Press, Woodbury, New York.

Peng, L., C. Shi, Z. Li, J.-P. Muller, J. Drummond, X. Li, T. Li, Y. Li, and J. Liu (2013), Evaluation of ASTER GDEM using GPS benchmarks and SRTM in China, *Int. J. Remote Sens.*, *34*(5), 1744–1771.

Philips, O. L., et al. (2009), Drought sensitivity of the Amazon rainforest, *Science*, *323*, 1344–1347.

Pokhrel, Y. N., N. Hanasaki, P. J. F. Yeh, T. J. Yamada, S. Kanae, and T. Oki (2012), Model estimates of sea level change due to anthropogenic impacts on terrestrial water storage, *Nat. Geosci.*, *5*, 389–392, doi:10.1038/ngeo1476.

Pokhrel, Y. N., Y. Fan, G. Miguez-Macho, P. J.-F. Yeh, and S.-C. Han (2013), The role of groundwater in the Amazon water cycle: 3. Influence on terrestrial water storage computations and comparison with GRACE, *J. Geophys. Res. Atmos.*, *118*, 3233–3244, doi:10.1002/jgrd.50335.

Potter, C., S. Klooster, C. Hiatt, V. Genovese, and J. C. Castilla-Rubio (2011), Changes in the carbon clycle of the Amazon ecosystem during the 2010 drought, *Environ. Res. Lett.*, *6*, doi:10.1088/1748-9326/6/3/034024.

Prigent, C., W. B. Rossow, and E. Matthews (1997), Microwave land surface emissivities estimated from SSM/I observations, *J. Geophys. Res.*, *102*, 21,867–21,890.

Prigent, C., E. Matthews, F. Aires, and W. B. Rossow (2001), Remote sensing of global wetland dynamics with multiple satellite datasets, *Geophys. Res. Lett.*, *28*, 4631–4634, doi:10.1029/2001GL013263.

Prigent, C., F. Aires, and W. B. Rossow (2006), Land surface microwave emissivities over the globe for a decade, *Bull. Am. Meteorol. Soc.*, *87*, 1573–1584, doi:10.1175/BAMS-87-11-1573.

Prigent, C., F. Papa, F. Aires, W. B. Rossow, and E. Matthews (2007), Global inundation dynamics inferred from multiple satellite observations, 1993-2000, *J. Geophys. Res.*, *112*, D12107, doi:10.1029/2006JD007847.

Prigent, C., F. Papa, F. Aires, C. Jimenez, W. B. Rossow, and E. Matthews (2012), Changes in land surface water dynamics since the 1990s and relation to population pressure, *Geophys. Res. Lett.*, *39*, L08403, doi:10.1029/2012GL051276.

Ramilien, G., S. Bouhours, A. Lombard, A. Cazenave, F. Flechtner, and R. Schmidt (2008), Land water storage contribution to sea level from GRACE geoid data over 2003–2006, *Global Planet. Change*, *60*, 381–392, doi:10.1016/j.gloplacha.2007.04.002.

Ramillien, G., F. Frappart, A. Cazenave, and A. Güntner (2005), Time variations of the land water storage from an inversion of 2 years of GRACE geoids, *Earth Planet Sci. Let.*, *235*, 283–301.

Richey, J., R. Meade, E. Salati, A. Devol, C. Nordin, and U. Dos Santos (1986), Water discharge and suspended sediment concentrations in the Amazon River: 1982–1984, *Water Resour. Res.*, *22*, 756–764.

Ringeval, B., N. de Noblet-Ducoudré, P. Ciais, P. Bousquet, C. Prigent, F. Papa, and W. B. Rossow (2010), An attempt to quantify the impact of changes in wetland extent on methane emissions at the seasonal and interannual time scales, *Global Biochem. Cycles*, *24*, GB2003, doi:10.1029/2008GB003354.

Ringeval, B., et al. (2012), Modelling sub-grid soil moisture saturation in the ORCHIDEE global land surface model: Evaluation against river discharges and remotely sensed data, *Geosci. Model Dev.*, *5*, 941–962, doi:10.5194/gmd-5-941-2012.

Rodell, M., J. Chen, H. Kato, J. Famiglietti, J. Nigro, and C. R. Wilson (2007), Estimating groundwater storage changes in the Mississippi river basin (USA) using GRACE, *Hydrogeol. J.*, *15*(1), 159–166, doi:10.1007/s10040-006-0103-7.

Rossow, W. B., and R. A. Schiffer (1999), Advances in understanding clouds from ISCCP, *Bull. Am. Meteorol. Soc.*, *80*, 2261–2287.

Santos Da Silva, J., F. Seyler, S. Calmant, O. C. R. Filho, E. Roux, A. A. Magalhães Araújo, and J.-L. Guyot (2012), Water level dynamics of Amazon wetlands at the watershed scale by satellite altimetry, *Int. J. Remote Sens.*, *33*(11), 3323–3353, doi:10.1080/01431161.2010.531914.

Schmidt, R., F. Flechtner, U. Meyer, K. H. Neumayer, C. Dahle, R. Koenig, and J. Kusche (2008), Hydrological signals observed by the GRACE satellites, *Surv. Geophys.*, *29*(4-5), 319–334, doi:10.1007/s10712-008-9033-3.

Sheffield, J., C. R. Ferguson, T. J. Troy, E. F. Wood, *and* M. F. McCabe (2009), Closing the terrestrial water budget from satellite remote sensing, *Geophys. Res. Lett.*, *36*, L07403, doi:10.1029/2009GL037338.

Smith, L. C. (1997), Satellite remote sensing of river inundation area, stage and processes: A review, *Hydrol. Processes*, *11*, 1427–1439.

Tapley, B. D., S. Bettadpur, J. C. Ries, P. F. Thompson, and M. Watkins (2004), GRACE measurements of mass variability in the Earth system, *Science*, *305*, 503–505.

Tomasella, J., L. S. Borma, J. A. Marengo, D. A. Rodriguez, L. A. Cuartas, C. A. Nobre, and M. C. R. Prado (2011), The droughts of 1996–97 and 2004–5 in Amazonia: Hydrological response in the river main-stem, *Hydrol. Process.*, *25*, 1228–1242.

Toutin, T. (2008), ASTER DEMs for geomatic and geoscientific applications: A review, *Int. J. Remote Sens.*, *29*, 1855–1875.

Valeriano, M. M., T. M. Kuplich, M. Storino, B. D. Amaral, J. N. Mendes Jr., and D. J. Lima (2006), Modeling small watersheds in Brazilian Amazonia with shuttle radar topographic mission-90 m data, *Comput. Geosci.*, *32*(8), 1169–1181.

Wania, R., et al. (2013), Present state of global wetland extent and wetland methane modelling: Methodology of a model intercomparison project (WETCHIMP), *Geosci. Model. Dev.*, *6*, 617–641, doi:10.5194/gmd-6-617-2013.

Wilson, M. D, P. D. Bates, D. Alsdorf, B. Forsberg, M. Horritt, J. Melack, F. Frappart, and J. Famiglietti (2007), Modelling large-scale inundation of Amazonian seasonally flooded wetlands, *Geophys. Res. Lett.*, *34*, L15404, doi:10.1029/2007GL030156.

Yamazaki, D., S. Kanae, H. Kim, and T. Oki (2011), A physically based description of floodplain inundation dynamics in a global river routing model, *Water Resour. Res.*, *47*, W04501, doi:10.1029/2010WR009726.

Yamazaki, D., C. A. Baugh, P. D. Bates, S. Kanae, D. E. Alsdorf, and T. Oki (2012), Adjustment of a spaceborne DEM for use in floodplain hydrodynamic modeling, *J. Hydrol.*, *436□437*, 81–91.